The Cotton-Mouton effect of furan and its homologues in gas phase and in solution: interplay of theory and experiment

Chiara Cappelli, Antonio Rizzo, Benedetta Mennucci, Jacopo Tomasi, Roberto Cammi, Rikken G.L.J.A., Renaud Mathevet, Carlo Rizzo

The Cotton–Mouton effect of furan and its homologues in the gas phase, for the pure liquids and in solution

Chiara Cappelli and Antonio Rizzo[a)]
Istituto per i Processi Chimico-Fisici (IPCF) del Consiglio Nazionale delle Ricerche, Via G. Moruzzi 1, I-56124, Pisa, Italy

Benedetta Mennucci and Jacopo Tomasi
Dipartimento di Chimica e Chimica Industriale dell'Università degli Studi di Pisa, Via Risorgimento 35, I-56126 Pisa, Italy

Roberto Cammi
Dipartimento di Chimica Generale ed Inorganica, Chimica Analitica, Chimica Fisica dell'Università di Parma, Parco Area delle Scienze 1, I-43100 Parma, Italy

Geert L. J. A. Rikken
Grenoble High Magnetic Field Laboratory, Max Planck Institut für Festkörperforschung/CNRS, BP 166, F-38042 Grenoble, France

Renaud Mathevet and Carlo Rizzo
LCAR-IRSAMC, Université Paul Sabatier et CNRS, 118, route de Narbonne, F-31062 Toulouse Cedex 04, France

The tensor components of the electric dipole polarizability at a wavelength of 632.8 nm, those of the magnetizability and the anisotropy of the static hypermagnetizability of furan, thiophene, and selenophene are computed using density functional theory (DFT). The polarizable continuum model (PCM) is employed to describe the system in the condensed phase. We can thus compare the temperature dependence of the Cotton–Mouton constant for the three molecules, both in the gas and in the condensed phase, pure liquids, and solutions, with the results of experiment performed using a 17 T radial access Bitter magnet at the Grenoble High Magnetic Field Laboratory. This allows to analyze, in a direct interaction of theory and experiment, the performance of DFT and PCM in describing high order nonlinear mixed electric and magnetic effects in condensed phase.

I. INTRODUCTION

The history of the Cotton–Mouton effect (CME) began almost exactly a century ago with the first observation of birefringence induced by a magnetic field on the radiation traversing condensed media, pure liquids, or solutions.[1,2] A complete theory of magnetic field induced birefringence came essentially in the mid-1950s, and it was due to Buckingham and Pople.[3] It was developed for ideal gases made of rigid, diamagnetic, noninteracting linear molecules, and it was accompanied by the first systematic measurements in gases.[4] It was only in the mid-1990s that progress in hardware, computational resources, and algorithms made it possible to perform *ab initio* accurate calculations of the intensity of the CME, essentially again in the gas phase—see Ref. 5 for a discussion of the field, both experiment and theory.

In spite of the fact that the experimental setup needed to determine the magnetic field induced birefringence in the gas phase is indubitably more complex—and the corresponding measurement more difficult—than needed for studies in condensed phase, the meeting of theory and experiment in this field has been quite rare. This is due, among other factors, to the complications arising in the theoretical description of optical properties in condensed fluids, as discussed by Buckingham in Ref. 6 in the context of electric field induced birefringence (Kerr effect). Properties measured in low-pressure gases and those derived from measurements in the liquid phase differ, as molecular interactions perturb the intrinsic polarizabilities, in the so-called solvent effect.

The state-of-the-art of the CME in liquids was discussed in 1993 in a review by Williams,[7] who refers essentially to his work with Torbet[8] as an example of experimental measurements of the CME of liquid water and of several aqueous solutions. That paper prompted, a few years later, interest in the computational study of the effect in liquid water, resulting in the analyses of Refs. 9 and 10, both involving one of the present authors (A.R.). In Ref. 9 a dielectric continuum model—with the solvated molecule placed in a spherical cavity and surrounded by a linear, homogeneous, polarizable dielectric medium—was employed for the description of the condensed phase. This led to an estimate of the Cotton–Mouton constant of liquid water differing in sign and by a factor of 8 in absolute value from that estimated by Williams and Torbet.[8] In Ref. 10 a semicontinuum model, where the central molecule was surrounded by its first solvation shell, was adopted. This improvement led to recovery of the cor-

a)Author to whom correspondence should be addressed; Electronic mail: rizzo@ipcf.cnr.it

rect sign of the effect, and reduced the discrepancy between absolute values to a factor of 3.

In the last few years it has been amply shown that continuum solvation models alone are not able to describe the properties of the solute in systems where an important net of hydrogen bonds (as, e.g., in the above-mentioned case of water in water) may be present.[11,12] As the study of Ref. 10 shows, a quantum mechanical description of the solvation cluster(s) may alleviate or eliminate the problem. The price to pay is that the solute plus solvent cluster is most often too large to be described appropriately at the high quantum mechanical level (including averages on the cluster motions) necessary for high order properties.

For these reasons we present here a CME study which for the computational part is based again on a continuum solvation model, applied however to systems in which no hydrogen bonds are present. The solvent effect is accounted for by resorting to the polarizable continuum model (PCM)[13,14] in its integral equation formalism (IEF) version.[15–17] Peculiarities of this solvation approach with respect to that used in Ref. 9 are (i) the use of realistic molecular cavities; (ii) the introduction of an apparent surface charge to describe the solute–solvent electrostatic interaction, and finally (iii) the accounting of the changes on the applied external field acting on the solute due to the presence of the solvent. In the PCM-IEF method the system is composed of two parts representing the system under study (a single molecule or an interacting cluster) and the environment. The system (usually indicated as the solute) is described as a quantum mechanical charge distribution within a volume, the so-called solute cavity, modeled on the molecular shape of the solute, and the environment (or the solvent) as a continuum dielectric. The solute polarizes the dielectric and the dielectric polarization in turn generates an electrostatic field at the solute, which modifies the original charge distribution.

In this paper we perform a complete computational study of the CME of furan, thiophene, and selenophene, both in gas and in the condensed phases, pure liquids and solutions. Dennis *et al.*[18] have presented some results of measurements of the infinite-dilution Cotton–Mouton constant of furan, thiophene, and selenophene as solutes in cyclohexane at 298 K and 632.8 nm. The measurements were coupled with those of the Kerr[19] and electric field gradient induced (EFGB)[20] birefringence constants and the analysis was mainly centered around the determination of molecular quadrupole moments. The association of Kerr, EFGB and Cotton–Mouton measurements aimed at determining electric and magnetic properties of molecules is a quite common occurrence not only in the condensed but also in the gas phase. The temperature dependence of the CME of furan and thiophene vapors has been determined experimentally by Coonan *et al.*,[21] in a study of the frequency dependent electric dipole polarizabilities where the authors compared the data obtained with those estimated computationally at Hartree–Fock self-consistent field or Møller–Plesset second-order level.

We compute the relevant molecular properties involved in the process, i.e., the tensor components of the frequency dependent electric dipole polarizability, $\alpha(\omega)$, of the magnetizability, ξ, and the anisotropy of the hypermagnetizability, $\Delta\eta$. A density functional theory approach that has proven to be very successful in a recent study of the CME of a series of di- and tri-atomic molecules in the gas phase[22] is employed. The effect has also been measured in the vapor (furan), in the pure liquids and in a few selected solutions of the target systems in common solvents, employing the state-of-the-art experimental apparatus available at the Grenoble High Magnetic Field Laboratory and which is equipped with a 17 T radial access Bitter magnet and a laser light beam operated at the wavelength of 632.8 nm.

In Sec. II we will go through the theory of the CME, giving emphasis to the aspect of solvent interactions and in particular to the use of PCM to compute electric and magnetic properties in condensed phase. A section briefly describing the experimental apparatus and techniques and outlining the relationships between theory and experiment follows. Computational details come next. We then present our results, both for the gas and the condensed phases, discussing connections between experiment and theory. A brief Conclusions section ends the paper.

II. THEORY

A. The Cotton–Mouton effect

When electromagnetic radiation of wavelength λ goes through a liquid or gaseous sample in a magnetic induction field B perpendicular to its direction of propagation it acquires an anisotropy of the refractive index induced by the field, $\Delta n(T,\lambda)=n_{\parallel}-n_{\perp}$, giving rise to an ellipticity. T indicates the temperature. $n_{\parallel}$ and $n_{\perp}$ are the refractive indices for light polarized at 0° and 90°, respectively, with respect to the direction of the applied field. The phase difference of the ray emerging from the interaction area whose length is l can be written as (radians)

$$\phi=2\pi C_{\mathrm{CM}}(T,\lambda)lB^2=\frac{2\pi l\Delta n(T,\lambda)}{\lambda}. \tag{1}$$

This is the so-called Cotton–Mouton effect (CME), and Eq. (1) introduces the Cotton–Mouton constant $C_{\mathrm{CM}}(T,\lambda)$. The "molar" Cotton–Mouton constant is defined by the relationship[7,23,24]

$${}_mC(T,\lambda)=\frac{2\lambda nC_{\mathrm{CM}}(T,\lambda)m(4\pi\epsilon_0)}{3(n^2+2)^2d}, \tag{2}$$

where d is the density, m the molar mass, and n the refractive index in absence of external magnetic induction. The dependence of the refractive index n on the wavelength has been neglected in Eq. (2) for sake of simplicity.

For an ideal gas made of rigid, noninteracting, diamagnetic molecules and for an uniform external field[3]

$$\Delta n(T,\lambda)=\frac{27B^2}{2V_m(4\pi\epsilon_0)}{}_mC(T,\lambda) \tag{3}$$

$$=\frac{\pi B^2N_A}{V_m(4\pi\epsilon_0)}[\Delta\eta(\lambda)+Q(T,\lambda)], \tag{4}$$

$$ {}_mC(T,\lambda) = \frac{2\pi N_A}{27}[\Delta\eta(\lambda) + Q(T,\lambda)], \tag{5} $$

$$ Q(T,\lambda) = \frac{1}{15kT}[3\alpha_{\alpha\beta}(\lambda)\xi_{\alpha\beta} - \alpha_{\alpha\alpha}(\lambda)\xi_{\beta\beta}]. \tag{6} $$

Here, V_m is the molar volume at a given pressure, N_A is Avogadro's number, k is the Boltzmann constant, and ϵ_0 is the permittivity of vacuum. The remaining quantities entering the equations are the tensor components of the frequency dependent electric dipole polarizability—$\alpha(\lambda)$, those of the magnetizability—ξ—and the anisotropy of the frequency dependent mixed electric and magnetic hypermagnetizability—$\eta(\lambda)$,

$$ \Delta\eta(\lambda) = \frac{1}{5}\sum_{\alpha,\beta}\left[\eta_{\alpha\beta,\alpha\beta}(\lambda) - \frac{1}{3}\eta_{\alpha\alpha,\beta\beta}(\lambda)\right]. \tag{7} $$

For a detailed discussion of the approximations made in deriving Eqs. (3)–(7) above the reader should refer to Refs. 3, 5, and 25.

The elements of the hypermagnetizability tensor of relevance for the Cotton–Mouton experiment, Eq. (7), can be shown to be related to a combination of quadratic and cubic frequency dependent response functions involving electric and magnetic dipole operators.[5] As for the frequency dependent electric dipole polarizability $\alpha(\lambda)$ and the magnetizability ξ, they can nowadays be computed quite efficiently resorting to modern analytic response theory[25,26] employing (multiconfigurational) self-consistent field wave functions. On the other hand an analytic approach that can guarantee magnetic gauge origin independence of the results for η is not yet available. One can then resort to a mixed numerical-analytic technique.[22,27] If the molecular energy ϵ in a magnetic induction (B) and an electric (E) field is expanded in power series, the static hypermagnetizability η can be identified as one of the mixed fourth-order derivatives or, equivalently, as a second derivative of either the magnetizability ξ or of the electric dipole polarizability α,[28]

$$ \eta = -\left.\frac{\partial^4\epsilon(B,E)}{\partial E^2\partial B^2}\right|_{B,E=0} = \left.\frac{\partial^2\xi(E)}{\partial E^2}\right|_{E=0} = \left.\frac{\partial^2\alpha(B)}{\partial B^2}\right|_{B=0}. \tag{8} $$

The next to last relationship defines the mixed numerical-analytic technique which can be exploited to evaluate the tensor elements of the hypermagnetizability. The frequency dependence of η is then neglected and the hypermagnetizability is evaluated by numerical differentiation of the analytically calculated magnetizabilities. The technique was first employed, in the context of CME, in Ref. 27 and used, in conjunction with DFT, in Ref. 22.

The computational effort is thus restricted to the determination of frequency dependent electric dipole polarizabilities $\alpha(\lambda)$ and magnetizabilities ξ, the last ones with and without the static electric field perturbation. To this end we employ a coupled-perturbed DFT approach.[29] Following the results of our recent analysis of the CME in small bi- and triatomic molecules in the gas phase,[22] we use a B3LYP hybrid functional, which performed excellently in Ref. 22 and which is the most widely used functional in the current literature. For a study of the performance of other popular density functionals the reader should refer to Ref. 22. Concerning the application of coupled-perturbed DFT for the calculation of frequency dependent electric dipole polarizabilities, see also Refs. 30–32.

Nowhere in this study do we attempt to determine or discuss the effect of molecular vibrations on the properties under study. The subject was discussed to some extent in Ref. 25, see also Ref. 5 and references therein, and Ref. 33.

B. Theory of magnetic field induced birefringence in solution: A PCM formulation

The "molar" Cotton–Mouton constant embodies the effects of the medium on the CME via the Lorentz–Lorenz approximation, assuming that the local optical field $\mathbf{E}^l$ acting at the solute site is related to the Maxwell optical field $\mathbf{E}$ by a local field factor,

$$ \mathbf{E}^l = \frac{n^2+2}{3}\mathbf{E}. $$

A more elegant and general formulation of the local field problem involves the introduction of the concept of "effective" molecular response properties, describing the response of the solute to the Maxwell field $\mathbf{E}$.[34–38] The approach relates directly the microscopic response polarizabilities to the macroscopic susceptibilities. Recently, we have proposed a protocol for the evaluation of "effective" molecular response properties within the framework of the PCM. It has been applied to the evaluation of the molar contribution to the refractive index and to nonlinear optical susceptibilities.[39–41] The extension to the Cotton–Mouton effect can be described as follows.

We define an "effective" molar Cotton–Mouton constant as

$$ \begin{aligned} {}_mC'(T,\lambda) &= {}_mC(T,\lambda)\frac{(n^2+2)^2}{9} \\ &= \frac{2\lambda n C_{\mathrm{CM}}(T,\lambda)m(4\pi\epsilon_0)}{27d} \\ &= \frac{2n(4\pi\epsilon_0)V_m}{27}\frac{\Delta n(T,\lambda)}{B^2}, \end{aligned} \tag{9} $$

$$ \Delta n(T,\lambda) = {}_mC'(T,\lambda)\frac{27B^2}{2nV_m(4\pi\epsilon_0)}, \tag{10} $$

which eliminates the Lorentz–Lorenz local field factor which enters Eq. (2). The effective molar Cotton–Mouton constant ${}_mC'$ can be directly related to the effective frequency dependent effective dipole polarizability $\tilde{\alpha}$, the magnetizability $\tilde{\xi}$, and the static hypermagnetizability $\tilde{\eta}$ by

$$ {}_mC'(T,\lambda) = \frac{2\pi N_A}{27}[\Delta\tilde{\eta}(\lambda) + \tilde{Q}(T,\lambda)], \tag{11} $$

$$ \tilde{Q}(T,\lambda) = \frac{1}{15kT}[3\tilde{\alpha}_{\alpha\beta}(\lambda)\tilde{\xi}_{\alpha\beta} - \tilde{\alpha}_{\alpha\alpha}(\lambda)\tilde{\xi}_{\beta\beta}], \tag{12} $$

$$\Delta\tilde{\eta}(\lambda)=\frac{1}{5}\sum\left[\tilde{\eta}_{\alpha\beta,\alpha\beta}(\lambda)-\frac{1}{3}\tilde{\eta}_{\alpha\alpha,\beta\beta}\right]. \quad (13)$$

The ''effective'' properties represent the solvent-modified response of the solute to the macroscopic electromagnetic fields **E** and **B**. Equation (11) can be obtained starting from the expression relating the squared refractive index n^2 and the effective electric dipole polarizability $\tilde{\pi}(\mathbf{B})$ in the presence of the magnetic field **B**,

$$\tilde{\pi}=\tilde{\alpha}+\tfrac{1}{2}\tilde{\eta}B^2+\cdots$$

and following the treatment of CME given by Buckingham and Pople in Ref. 3. In terms of $\tilde{\pi}(\mathbf{B})$ we directly obtain the response of the system to the Maxwell fields exactly as for dilute gases, and thus avoid the introduction of scaling factors usually needed in previous treatments of response properties for condensed systems.[42]

In this paper the effective polarizability and all the other quantities of Eqs. (10)–(13) will be calculated within the PCM-IEF continuum solvation model. The PCM-IEF theory for the analytic calculation of both $\tilde{\alpha}$ and $\tilde{\xi}$ has already been presented in Refs. 39–41 and Ref. 43, whereas for $\tilde{\eta}$ we resort to a mixed numerical-analytic technique exactly as for the isolated system

$$\tilde{\eta}=\frac{\partial^2\tilde{\xi}}{\partial^2 E}. \quad (14)$$

The calculation of the frequency dependent effective polarizability entering Eq. (12) involves two important solvent-specific aspects.

The first feature appears any time an oscillating external field is applied: in this case the field originates in the solute electronic charge distribution oscillations which may induce a delay in the response of the solvent. When the time scales of such oscillations are much shorter than the time scale of the solvent inertial response a nonequilibrium solute–solvent regime arises. In the PCM-IEF framework, the nonequilibrium is realized by evaluating the solvent charges in terms of the optical dielectric constant instead of the static analog.[44–48]

The second aspect is the modification of the external field acting at the solvated–solute site due to the presence of the solvent molecules (the phenomenon is historically indicated as a local field effect and it can be partitioned in ''reaction'' and ''cavity'' field parts).[49,42] As said earlier, in the PCM-IEF framework the problem is solved by introducing effective quantities which, together with the reaction charges, allow one to directly relate the response of the solute to the external macroscopic field exactly as in gas phase but still including the local field effects.[39–41]

In particular when the applied field is an oscillating electric field, the time-dependent perturbation $\hat{V}'(t)$ to be included in the Hamiltonian can be represented as

$$\hat{V}'(t)=(\hat{\mu}_\alpha+\tilde{\mu}_\alpha)E_\alpha(e^{i\omega t}+e^{-i\omega t}), \quad (15)$$

where Einstein summation over repeated indices is implied and $\hat{\mu}$ is the electric dipole operator. The additional solvent-induced dipole operator $\tilde{\mu}$ takes into account effects due to the field generated from the response of the solvent to the probing field once the cavity has been created (the so-called ''cavity field'' part of the local field effect).

In the density functional formalism for a one-determinant wave function with orbital expansion over a finite basis set, the Fock matrix to be inserted in the corresponding time-dependent Kohl–Sham (TDKS) equation becomes

$$\mathbf{F}'=\mathbf{F}^{\mathrm{sol}}+\sum_\alpha\left[\mathbf{m}_\alpha+\tilde{\mathbf{m}}_\alpha(\omega)\right]E_\alpha(e^{i\omega t}+e^{-i\omega t}), \quad (16)$$

where $\mathbf{F}^{\mathrm{sol}}$ is the Fock matrix of the solute without the applied field but including the ''reaction'' field effects due to the solvent. $\mathbf{m}_\alpha$ collects the integrals of the αth Cartesian component of the dipole moment operator. $\tilde{\mathbf{m}}_\alpha(\omega)$ is the matrix form of the cavity-field operator $\tilde{\mu}_a$ introduced in Eq. (15) (the exact definition of $\tilde{\mathbf{m}}$ can be found in Refs. 39–41).

By solving the corresponding TDKS equation

$$\mathbf{F}'\mathbf{C}-i\frac{\partial}{\partial t}\mathbf{SC}=\mathbf{SC}\boldsymbol{\epsilon} \quad (17)$$

with the proper orthonormality condition, the density matrix derivative $\tilde{\mathbf{R}}^\beta(\omega)$ with respect to any component of the external electric field **E** is obtained. In Eq. (17) **S** represents the overlap matrix, **C** the matrix collecting the MO coefficients, and $\boldsymbol{\epsilon}$ the orbital energies.

Approximate solutions of the time-dependent equation (17) can be obtained using the same algorithm formulated for isolated molecules.[50] Once $\tilde{\mathbf{R}}^\beta(\omega)$ is known, the effective polarizability $\tilde{\alpha}$ can be obtained as

$$\tilde{\alpha}_{\alpha\beta}(-\omega;\omega)=-\mathrm{Tr}[\mathbf{m}_\alpha\tilde{\mathbf{R}}^\beta(\omega)] \quad (18)$$

Note that $\tilde{\alpha}$ is computed by considering, in the nonequilibrium framework, both the solvent response to the molecular charge distribution and the solvent response to the external electric field.

In the present work the continuous set of gauge transformations (CSGT) formalism is applied[51–53] to compute the magnetizability ξ, the second-order function which describes the response of the solute to an external magnetic field **B**. In this approach the magnetic susceptibility is obtained in terms of the first-order induced electronic current $J(\mathbf{B})$. Gauge invariance is assured by performing an accurate calculation of the induced electronic current with a gauge transformation introduced at each point in space. $J(\mathbf{B})$ is computed from the first-order correction to the molecular orbitals through a specific coupled perturbed Kohn–Sham (CPKS) scheme. The calculation of the magnetizability within PCM-IEF in the CSGT formalism has been presented in Ref. 43. In this case, contrary to what happens for electric-field perturbations, the PCM contribution explicitly affects only the unperturbed equations, as no solvent dependent term appears in the first-order correction. Here the external magnetic field is supposed to be static, and thus an equilibrium solvent response will be used. In addition, no magnetic cavity effects will be considered.

III. EXPERIMENTAL SETUP

A general introduction to experimental techniques employed to measure the CME can be found in Ref. 5.

The experimental setup used to measure the Cotton–Mouton effect is made available to users by the High Magnetic Field Laboratory in Grenoble. The apparatus has been operating since the early 1980s[54] and it is described in detail in Ref. 55, where it was used to demonstrate the existence of a linear birefringence induced by the application of both an electric and a magnetic induction field (magnetoelectric birefringence) in a liquid molecular sample. This optical effect is essentially the same as that observed in the case of CME, the main difference being that magnetoelectric birefringence is bilinear in the two external fields, whereas the CME displays a quadratic dependence on the strength of the magnetic induction field. The apparatus is essentially based on a HeNe laser operating at a wavelength of 632.8 nm and whose light beam is polarized and sent through a region where both a transverse magnet field and the liquid sample are present. The latter is placed in a 3-cm-long cuvette with low birefringence quartz windows. The magnetic field is generated by a 17 T radial access Bitter magnet. This strength is one of the highest available in the Voigt configuration, i.e., designed for measurements of birefringences such as those observed in the CME. For the liquid measurements the field was homogeneous within 1% across the sample. The apparatus was originally designed and is thus optimized for measurements made in solids or liquids. With such an arrangement the beam propagates in air before reaching the sample, placed in the center of the magnet, where the temperature is measured. For measurements made on the vapor the apparatus had to be modified by adding windows at the extremities of the magnet, in order to allow for the whole magnet bore to be filled with the gas at a known temperature and pressure. The calculated field profile along the radial magnet bore was used to convert the observed linear birefringence into the Cotton–Mouton constant. The polarization of the light after the magnet was then analyzed by a polarizer crossed with respect to the initial polarization of the beam. The use of a photoelastic ellipticity modulator after the first polarizer allows the use of a phase sensitive detection technique to measure the resulting birefringence. Calibration of the birefringence was performed with a quartz Babinet–Soleil compensator. For our measurements the field was swept between 0 and 17 T in runs lasting a few seconds, while monitoring the ellipticity, which is a linear function of the squared field amplitude. The slope of this function is proportional to the CME. For measurements in condensed phases a good reproducibility, corresponding to a few percent error bar, could be obtained. This was not the case for the measurements made on the vapor phase, probably due to the fact that the gas filling the whole magnet bore ended up being directly in contact with it and measurements were likely affected by temperature and pressure gradients. The data obtained in the vapor phase, and whose error bars include those of the values already existing in the literature (*vide infra*), should be considered as obtained in the calibration procedure of the whole apparatus.

The relationship between the molecular Cotton–Mouton constant measured in solution C_{CM} [definition in Eq. (1), we drop here for sake of simplicity the explicit dependence on T and λ] and the molar ${}_mC$ Cotton–Mouton constant extrapolated at infinite dilution were discussed by William,[7] who refers to the work of LeFèvre and co-workers.[23,24] Here C_{CM} in solution was determined as the infinite dilution limit of a series of measurements at different low concentrations of the given solute in each solvent. For a mixture made of n_{solute} moles of the solute and n_{solvent} moles of the solvent, assuming ideal behavior and taking, in the limit of infinite dilution, $V^{(\mathrm{solution})} \approx n_{\mathrm{solvent}} V_m^{(\mathrm{solvent})}$, the following relationship holds:[7]

$$C_{\mathrm{CM}}^{(\mathrm{solution})} \approx C_{\mathrm{CM}}^{(\mathrm{solvent})} + c_{\mathrm{solute}} \times V_m^{(\mathrm{solvent})} \times [C_{\mathrm{CM}}^{(\mathrm{solute})} - C_{\mathrm{CM}}^{(\mathrm{solvent})}], \tag{19}$$

where $C_{\mathrm{CM}}^{(\mathrm{solute})}$ indicates the Cotton–Mouton constant of the solute at infinite dilution, $C_{\mathrm{CM}}^{(\mathrm{solvent})}$ that of the pure solvent, and c_{solute} indicates the concentration (number of moles per volume) of the solute in the solution. Typical results of our measurements of $C_{\mathrm{CM}}^{(\mathrm{solution})}$ are shown in Figs. 1–3. In Fig. 1 $C_{\mathrm{CM}}^{(\mathrm{solution})}$ is reported as a function of the molar concentration for the case of solutions of furan in cyclohexane, CCl_4, and acetone. Measurements were made at a wavelength of 632.8 nm and a temperature of 293.15 K. For the same wavelength and temperature, Fig. 2 displays the results obtained for solutions of thiophene in cyclohexane and in acetone, whereas Fig. 3 shows the corresponding data for selenophene. In all cases considered, a linear concentration dependence at sufficiently low concentrations was observed, whereas for some cases, deviations at high concentrations were observed, see, e.g., Figs. 2 and 3.

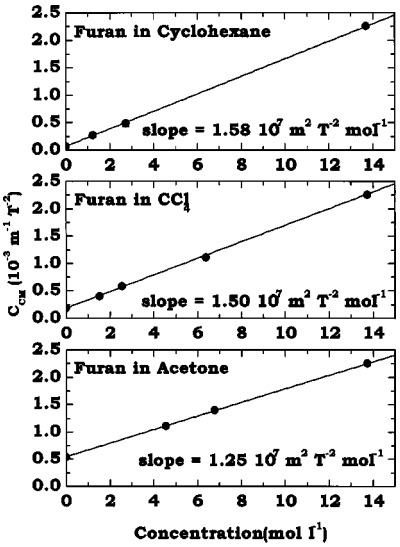

FIG. 1. C_{CM} [definition in Eq. (1)] as a function of the molar concentration for the case of solutions of furan in cyclohexane, acetone, and CCl_4 at a wavelength of 632.8 nm and a temperature of 293.15 K.

For a given combination of solute and solvent, the slope of the fitting line was divided, according to Eq. (19), by the molar volume of the solvents, V_m^{solvent}, obtained as the inverse of the concentration of the solvents as pure liquid ($V_m^{(\mathrm{solvent})} = 1/c_{\mathrm{solvent}}^{\mathrm{pl}}$), and then added to the intercept ($C_{\mathrm{CM}}^{(\mathrm{solvent})}$) to yield $C_{\mathrm{CM}}^{(\mathrm{solute})}$. Estimates of the concentration of the pure solvent $c_{\mathrm{solvent}}^{\mathrm{pl}}$ were obtained from its molecular

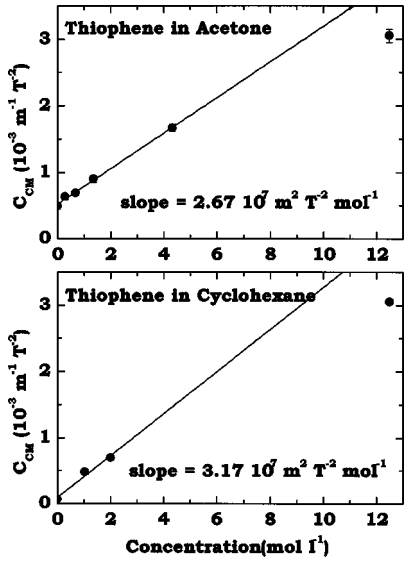

FIG. 2. C_{CM} [definition in Eq. (1)] as a function of the molar concentration for the case of solutions of thiophene in cyclohexane and acetone, at a wavelength of 632.8 nm and a temperature of 293.15 K.

weight and data for the density at 293.15 K taken from Refs. 56 and 57. In Secs. V B and V C the comparison between experimental and *ab initio* results is made through the values of $\Delta n_l(T,\lambda)$, which corresponds to the anisotropy, see Eq. (10), observed for the solute at infinite dilution in a magnetic field induction field intensity of 1 T. To obtain Δn_l from the data of the experiment we employ

$$\Delta n_l(T,\lambda)=\lambda B^2 \;\; C_{\mathrm{CM}}^{(\mathrm{solute})}|_{B=1\ \mathrm{T}}, \tag{20}$$

whereas the *ab initio* estimate is obtained exploiting [see Eqs. (10) and (11)]

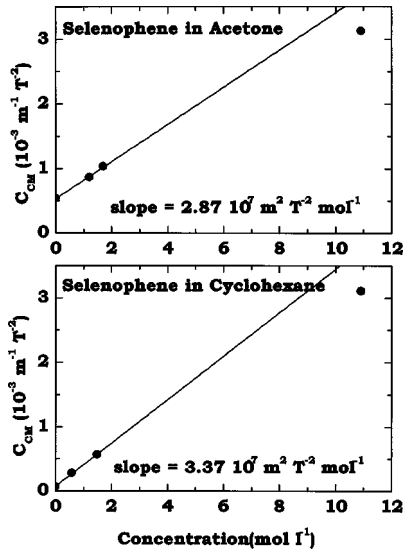

FIG. 3. C_{CM} [definition in Eq. (1)] as a function of the molar concentration for the case of solutions of selenophene in cyclohexane and acetone, at a wavelength of 632.8 nm and a temperature of 293.15 K.

$$\Delta n_l(T,\lambda)=\frac{\pi N_A B^2}{n(4\pi\epsilon_0)V_m^{\mathrm{solvent}}}[\Delta\tilde{\eta}(\lambda)+\tilde{Q}(T,\lambda)]|_{B=1\ \mathrm{T}}$$
$$=\frac{\pi N_A B^2 c_{\mathrm{solvent}}^{\mathrm{pl}}}{n(4\pi\epsilon_0)}[\Delta\tilde{\eta}(\lambda)+\tilde{Q}(T,\lambda)]|_{B=1\ \mathrm{T}}. \tag{21}$$

The highest concentrations in Figs. 1–3 correspond to measurement made in the pure (solute) liquids. They yield directly, through Eq. (20), the data for $\Delta n_l(T,\lambda)$ of pure liquid furan, thiophene, and selenophene.

Systematic uncertainties of the measurements made in solution can be estimated to be of the order of 5%. The choice and the number of the gas and solution samples employed in the measurements was essentially determined by the magnet time allocated to the experimentalists.

IV. COMPUTATIONAL DETAILS

All the calculations were performed at the DFT level with the hybrid B3LYP functional and using Dunning's correlation consistent sets. For the calculations on furan in the gas phase we have employed four sets ranging from the aug-cc-pVDZ to the d-aug-cc-pVTZ, in order to study the convergence of the properties with the increase of the basis. For the calculations in the condensed phase, which are more computationally intensive and involve several solvents, we have limited our study to the d-aug-cc-pVDZ basis set for furan and thiophene, and to the aug-cc-pVDZ set for selenophene. Unless where explicitly stated (see Sec. V) the geometries of all the systems have been kept fixed to the corresponding experimental values for the gas-phase systems, see Ref. 58 for furan, Ref. 59 for thiophene, and Ref. 60 for selenophene.

The polarizabilities and magnetizabilities were computed by using a CPKS approach.[29–32,22] For a coherent comparison with experiment the frequency dependence was explicitly taken into account in the calculation of polarizabilities (λ=632.8 nm).

Following our previous studies[22,25] an electric field strength of 0.007 a.u. was used to calculate the hypermagnetizabilities as numerical derivatives of the magnetizabilities [see Eqs. (7), (8), (13), and (14)]. This strength ensured a good numerical stability of the results. Note that the approach involves several calculations with different field setups, in most cases with symmetry lower than that of the system in absence of an external field.

The PCM calculations were performed using molecular cavities made of interlocking spheres centered on the heavy atoms (globally we have five spheres for each of the three systems). The radii of the spheres have been deduced from the van der Waals radii multiplied by a cavity size factor of 1.2, namely $R_x=R_{\mathrm{vdW}}\times 1.2$. In this scheme the radii centered on the carbon atoms, and including an hydrogen atom, were put equal to 2.28 Å, whereas those on the heteroatoms were derived from Bondi's R_{vdW}.[61] They are: $R_{\mathrm{O}}=1.824$ Å, $R_{\mathrm{S}}=2.16$ Å, and $R_{\mathrm{Se}}=2.28$ Å. The static (ϵ) and optical (n) dielectric constants employed in the calculations are given in Tables III–VI.

TABLE I. Furan and thiophene. B3LYP/d-aug-cc-pVDZ and experimental gas-phase results (in a.u., except where otherwise specified). Molecules on xz plane. $\lambda=632.8$ nm.

	Furan		Thiophene	
	Calc.	Expt.	Calc.	Expt.
α_{xx}	61.25[a]	59.2±2.5[b]	73.93	71.0±6.1[b]
α_{yy}	36.06[a]	34.9±0.8[b]	45.66	44.2±2.8[b]
α_{zz}	55.21[a]	53.3±2.2[b]	80.37	79.5±4.9[b]
α_{iso}[c]	50.84	49.1±0.5[d]	66.65	64.9±0.6[d]
$\xi_{xx}-\xi_{\mathrm{iso}}$[e]	2.45	2.41±0.01[f]	3.72	3.55±0.09[f]
$\xi_{yy}-\xi_{\mathrm{iso}}$	−5.60	−5.44±0.03[f]	−7.35	−7.03±0.11[f]
$\xi_{zz}-\xi_{\mathrm{iso}}$	3.14	3.02±0.01[f]	3.63	3.47±0.08[f]
$\Delta\eta$	−18.14	$(3.4\pm1.0)\times10^{3}$ [b]	82.32	$(6.0\pm8.4)\times10^{3}$ [b]
$10^{17}\times{}_{m}C(292.15\ \mathrm{K},\lambda)$[g]	9.91	9.52±0.13[h] 11±2[i]	18.81	18.1±1.0[h]
$10^{12}\times\Delta n_{u}(292.15\ \mathrm{K},\lambda)$[j]	5.58	5.36±0.07[h] 6.2±1.2[i]	10.59	10.2±0.6[h]

[a]Best estimates at 632.8 nm from Ref. 63, coupled-cluster response: $\alpha_{xx}=58.3(9)$; $\alpha_{yy}=35.1(4)$; $\alpha_{zz}=53.9(9)$.
[b]Reference 21.
[c]$\alpha_{\mathrm{iso}}=\frac{1}{3}(\alpha_{xx}+\alpha_{yy}+\alpha_{zz})$.
[d]See Ref. 21; cited as taken from data for the pure liquid, Ref. 18.
[e]$\xi_{\mathrm{iso}}=\frac{1}{3}(\xi_{xx}+\xi_{yy}+\xi_{zz})$.
[f]See Ref. 21; cited as taken from Ref. 65.
[g]In $\mathrm{cm^3\ G^{-2}\ mol^{-1}}(4\pi\epsilon_0)$.
[h]Reference 21. From the data of P and Q given in Table III, p. 7303.
[i]This work. Field induction of 1 T, pressure of 1 atm, temperature of 19°, $\lambda=632.8$ nm.
[j]$\Delta n_{u}(T,\lambda)=\Delta n(T,\lambda)\big|_{B=1\ \mathrm{T},P=1\ \mathrm{atm}}$.

The CPKS calculations were performed using a development version of the GAUSSIAN code.[62]

V. RESULTS

A. Gas phase

In Table I we report the B3LYP/d-aug-cc-pVDZ results obtained for furan and thiophene in the gas phase. Data for the anisotropy of the refractive index are given as $\Delta n_{u}(T,\lambda)$, the anisotropy measured with a magnetic field induction field intensity of 1 T and with the (ideal) gas kept at a pressure of 1 atm.[5] Existing experimental reference data are taken from Ref. 21. For furan a new experimental value of the magnetic field induced anisotropy and of the corresponding molar Cotton–Mouton constant measured in the course of this study is given. Again for the specific case of furan, Table II shows the dependence of the properties on the basis set and can be used to discuss the effect of optimizing explicitly the geometry *in vacuo*. Let us turn our attention to this table first.

The tensor elements show a good stability with the change of size and quality of the basis set for both the frequency dependent electric dipole polarizability and the magnetizability. The increase in the cardinal number changes the former by about 3% and the latter by roughly 1%. As far as the electric dipole polarizability is concerned, augmentation has an opposite effect on the double zeta and triple zeta sets, respectively. d-aug-cc-pVDZ results are ≈0.5% to ≈1% larger than the corresponding aug-cc-pVDZ results. The effect of double augmentation is more substantial (≈2.5% to ≈3%) at triple zeta level, and opposite, leading to a decrease of the magnitude of the tensor elements. The stability of the magnetizability is rather remarkable: double augmentation affects the tensor elements by a fraction of a percent, whereas changes are on the order of a few ppm at triple zeta level.

It is no surprise that the anisotropy of the hypermagnetizability shows a stronger dependence on the basis set: doubly augmenting the basis at DZ level decreases $\Delta\eta$ by ≈15%. Increasing the cardinal number also decreases $\Delta\eta$, by ≈10%. The calculation of the anisotropy, carried out as indicated in Sec. II A via numerical differentiation of the magnetizability tensor elements in finite electric fields, becomes rather expensive when employing the d-aug-cc-pVTZ set, and it was not attempted. On the other hand, as is quite usual in the study of birefringences, its contribution to the observable at 292.15 K is very small, of 600–800 ppm with respect to that of the Langevin term $Q(T,\lambda)$, and thus inaccuracies on $\Delta\eta$ of the order of those likely to be associated with the numbers in Tables I and II have no influence on the overall observable.

In Table II a comparison is also made between the results obtained using the d-aug-cc-pVDZ basis set on two different geometrical setups: the experimental arrangement (employed as standard throughout the paper, see Sec. IV) and the geometry resulting from a B3LYP/d-aug-cc-pVDZ optimization *in vacuo*. The largest variation, occurring again on the anisotropy of the hypermagnetizability, is of the order of 4%–5%, whereas on average the lower order properties (electric dipole polarizability and magnetizability) do not change more that ≈1%.

In Table I we report the results of the calculations on furan and thiophene performed using the d-aug-cc-pVDZ ba-

TABLE II. Basis set dependence of the gas-phase results in furan. B3LYP. Molecule on the xz plane. λ=632.8 nm. Atomic units except where otherwise indicated.

	aug-cc-pVDZ	d-aug-cc-pVDZ	aug-cc-pVTZ	d-aug-cc-pVTZ	d-aug-cc-pVDZ[a]
α_{xx}	60.58	61.25	61.06	58.97	61.98
α_{yy}	35.81	36.06	36.03	35.15	36.34
α_{zz}	54.93	55.21	55.10	53.63	55.86
$\alpha_{\rm iso}$[b]	50.44	50.84	50.73	49.25	51.40
ξ_{xx}	−6.62	−6.61	−6.62	−6.62	−6.63
ξ_{yy}	−14.63	−14.66	−14.83	−14.83	−14.69
ξ_{zz}	−5.91	−5.93	−5.97	−5.97	−5.97
$\xi_{\rm iso}$[c]	−9.05	−9.07	−9.14	−9.14	−9.09
$[\alpha\xi]$[d]	361.30	365.98	370.63	356.24	372.79
$10^{-3}\times Q(292.15\ {\rm K},\lambda)$	26.03	26.37	26.71	25.67	26.86
$\Delta\eta$	−21.15	−18.14	−19.00	−19.00[e]	−17.30
$10^{17}\times {}_mC(292.15\ {\rm K},\lambda)$[f]	9.78	9.91	10.03	9.64	10.09
$10^{12}\times \Delta n_u(292.15\ {\rm K},\lambda)$[g]	5.51	5.58	5.65	5.43	5.68

[a]Geometry optimized *in vacuo*.
[b]$\alpha_{\rm iso}=\frac{1}{3}(\alpha_{xx}+\alpha_{yy}+\alpha_{zz})$.
[c]$\xi_{\rm iso}=\frac{1}{3}(\xi_{xx}+\xi_{yy}+\xi_{zz})$.
[d]$[\alpha\xi]=[(\alpha_{xx}-\alpha_{yy})\cdot(\xi_{xx}-\xi_{yy})+(\alpha_{yy}-\alpha_{zz})\cdot(\xi_{yy}-\xi_{zz})+(\alpha_{zz}-\alpha_{xx})\cdot(\xi_{zz}-\xi_{xx})]=3[\alpha_{xx}\cdot(\xi_{xx}-\xi_{\rm iso})+\alpha_{yy}\cdot(\xi_{yy}-\xi_{\rm iso})+\alpha_{zz}\cdot(\xi_{zz}-\xi_{\rm iso})]$.
[e]Assumed equal to the value yielded by the aug-cc-pVTZ basis set, see the text.
[f]In cm^3 G^{-2} mol^{-1}($4\pi\epsilon_0$).
[g]$\Delta n_u(T,\lambda)=\Delta n(T,\lambda)|_{B=1\ {\rm T},P=1\ {\rm atm}}$.

sis set, as for these two molecules experimental literature references exist both for the individual properties (electric dipole polarizability, magnetizability) and for the CME itself. These are mainly directly taken from, or reported in, the study by Coonan and co-workers of Ref. 21. We have also carried out the calculation of the CME of selenophene employing the aug-cc-pVDZ basis set, obtaining (for a wavelength of 632.8 nm and assuming a temperature of 292.15 K) the following results: $\alpha_{\rm iso}=74.04$ a.u.; $\xi_{\rm iso}=-13.82$ a.u.; $\Delta\eta=191.14$ a.u.; ${}_mC(292.15\ {\rm K},\ 632.8\ {\rm nm})=20.59\times10^{-17}$ cm^3 G^{-2} ($4\pi\epsilon_0$); $\Delta n_u(292.15\ {\rm K},\ 632.8\ {\rm nm})=11.59\times10^{-12}$. As no experimental data appear to be available for this molecule in the literature, the numbers were not included in Table I and we do not discuss them any further.

The performance of DFT is excellent, as proven by the agreement between our data for both the electric dipole polarizability and the magnetizability (both tensor components and averages) and the experiment, which in some cases are derived from data taken from measurements made in the liquid phase (see Table I). In all cases our polarizability tensor components fall within less than three error bars of the experiment. Experimental error bars are extremely tight for the magnetizability, where nonetheless agreement remains more than satisfactory, especially for thiophene. In Ref. 22 we have already shown how satisfactorily B3LYP/DFT can perform in the calculation of the magnetizability tensor with respect to other more expensive and delicate *ab initio* approaches, such as complete active space self-consistent field.

In the case of furan, we can also appreciate the efficiency of B3LYP/DFT by comparing our results with those of the sophisticated state-of-the-art calculation carried out by Christiansen and co-workers,[63] who performed a coupled cluster calculation of the polarizability of furan, using a hierarchy of models ranging up to coupled cluster singles and doubles.

There is no need to spend too many words in discussing the relationships between theory and experiment as far as the anisotropy of the hypermagnetizability is concerned. The huge error bar resulting from the extremely delicate infinite temperature extrapolation attempted by experimentalists leaves plenty of space for agreement in the case of thiophene, whereas the computed datum for furan lies outside three times the error bar associated with experiment. The important point is the excellent agreement between theory and experiment for the overall observable, the Cotton–Mouton constant or, more directly, the anisotropy of the refractive index, $\Delta n_u(T,\lambda)$. For the latter we compute $\Delta n_u(292.15\ {\rm K},\ 632.8\ {\rm nm})=5.58\times10^{-12}$ and $\Delta n_u(292.15\ {\rm K},\ 632.8\ {\rm nm})=10.59\times10^{-12}$, for gaseous furan and thiophene, respectively, in both cases within or very close to three times the error bars (representing single standard deviations) of the experiment, both that of Ref. 21 and (for furan) our own. This is an extremely satisfactory result considering the numerous approximations (see, e.g., the relatively limited basis set, the in principle unsophisticated treatment of electron correlation, the neglect of vibrational contributions, the uncertainty arising from the neglect of intermolecular interactions in the theoretical treatment and that inherent in the extrapolation made to zero gas density in the experiment).

B. Pure liquids

In Table III we report the results computed for furan, thiophene, and selenophene as pure liquids and compare with experiment. Here and in the following section the level of the

TABLE III. B3LYP/d-aug-cc-pVDZ and experimental results (a.u.) for furan, thiophene, and selenophene as pure liquids. Molecule on xz plane. λ=632.8 nm.

	Furan	Thiophene	Selenophene
n^2	2.02	2.337	2.496
ϵ	2.95	2.76	2.6
$\tilde{\alpha}_{xx}$	78.50	101.08	111.96
$\tilde{\alpha}_{yy}$	49.48	67.63	77.92
$\tilde{\alpha}_{zz}$	72.22	111.81	130.93
$\tilde{\alpha}_{iso}$	66.73	93.51	106.94
$\tilde{\alpha}_{\rm iso}$(exp)[a]	65.10	94.15	122.84
ξ_{xx}	−6.62	−8.36	−10.02
ξ_{yy}	−14.66	−19.44	−21.10
ξ_{zz}	−5.88	−8.42	−10.27
$\xi_{\rm iso}$	−9.05	−12.07	−13.80
$\xi_{\rm iso}$(exp)[b]	−9.068	−12.07	−14.06
$[\tilde{\alpha}\xi]$[c]	428.33	856.85	946.80
$10^{-3}\times Q(293.15\ \mathrm{K},\lambda)$	30.76	61.53	67.99
$\Delta\eta$	−19.84	96.58	216.97
$10^9\times\Delta n_l(293.15\ \mathrm{K},\lambda)$[d]	1.53	2.59	2.38
$10^9\times\Delta n_l(293.15\ \mathrm{K},\lambda)$(exp)[d]	1.42	1.93	1.97

[a]Estimated from refractive index and density data using the Lorentz–Lorenz formula (see the text and Ref. 66) and the values of density given in Refs. 56 and (for selenophene) 57.
[b]Reference 56.
[c]$[\tilde{\alpha}\xi]=[(\tilde{\alpha}_{xx}-\tilde{\alpha}_{yy})\cdot(\xi_{xx}-\xi_{yy})+(\tilde{\alpha}_{yy}-\tilde{\alpha}_{zz})\cdot(\xi_{yy}-\xi_{zz})+(\tilde{\alpha}_{zz}-\tilde{\alpha}_{xx})\cdot(\xi_{zz}-\xi_{xx})]=3[\tilde{\alpha}_{xx}\cdot(\xi_{xx}-\xi_{\rm iso})+\tilde{\alpha}_{yy}\cdot(\xi_{yy}-\xi_{\rm iso})+\tilde{\alpha}_{zz}\cdot(\xi_{zz}-\xi_{\rm iso})]$.
[d]See the definition in Eq. (20).

calculations is B3LYP/d-aug-cc-pVDZ for furan and thiophene and B3LYP/aug-cc-pVDZ for selenophene.

As far as the isotropic polarizability $\tilde{\alpha}_{\rm iso}$ is concerned, we note that an estimate for pure liquids can be derived from the experimental data for the refractive index n by resorting to the Lorentz–Lorenz formula

$$(n^2-1)=\frac{N_A d}{\epsilon_0 M_w}\tilde{\alpha}_{\rm iso},$$

where d again denotes the density of the liquid and M_w is the molecular weight. We obtain for $\tilde{\alpha}_{\rm iso}$ estimates of 65.10 a.u. for furan, 94.15 a.u. for thiophene, and 122.84 a.u. for selenophene. This last estimate was obtained assuming for selenophene a density at 20° of 1.423 g ml^{-1}, that of commercially available selenophene.[57] Our calculated results for furan and thiophene are in excellent agreement with these numbers, the difference between experiment and calculation being less than 1%. The comparison is less favorable for selenophene, with a difference of ≈13%. This is not surprising, since in this case we employed a singly augmented correlation consistent basis set. The same holds for $\xi_{\rm iso}$, the difference between calculated and experimental values being less than 0.2% for furan and thiophene and ≈1.8% for selenophene.

As far as $\Delta n_l(T,\lambda)$ is concerned, the calculated results are quite good for furan but less satisfactory for thiophene and selenophene. This different behavior can be ascribed to the specific nature of the three systems. In particular, for thiophene and selenophene possible aggregation effects, not reproduced by the PCM theoretical model, which is based on an average solvation, are likely to be responsible for the disagreement. Further evidence comes from the deviation from linearity observed for the molar Cotton–Mouton constant of pure liquid thiophene and selenophene for the solutions in Figs. 2 and 3. Furan's behavior (Fig. 1) is in this respect very close to ideality, with no deviation from linearity observable in our measurements. The fact that the comparison between computed and measured isotropic polarizability and magnetizability is more satisfactory than seen for $\Delta n_l(T,\lambda)$ strengthens the idea that the discrepancy is due to specific (aggregation) effects. This type of effect is indeed much less important for isotropic quantities than for a property like $\Delta n_l(T,\lambda)$, heavily involving anisotropic responses.

C. Solutions

Tables IV–VI display the results obtained for each of the three homologues in solutions involving different solvents (cyclohexane, CCl_4, THF, acetone, acetonitrile, and dimethylformamide).

Looking at the trend of $\Delta n_l(T,\lambda)$ going from apolar to increasingly polar solvents, we observe that the calculated results reproduce with sufficient accuracy the observed trends, even if the size of solvent effects is sometimes underestimated.

As far as the trend within the three homologues (furan, thiophene, selenophene) is concerned, the calculated results correctly describe the increase of $\Delta n_l(T,\lambda)$ going from furan to thiophene (and selenophene), see, for instance, in cyclohexane: $\Delta n_l(293.15\ \mathrm{K},\ 632.8\ \mathrm{nm})=1.02\times10^{-9}$ (furan), $\Delta n_l(293.15\ \mathrm{K},\ 632.8\ \mathrm{nm})=1.99\times10^{-9}$ (thiophene), $\Delta n_l(293.15\ \mathrm{K},\ 632.8\ \mathrm{nm})=2.18\times10^{-9}$ (selenophene) measured versus $\Delta n_l(293.15\ \mathrm{K},632.8\ \mathrm{nm})=0.98\times10^{-9}$ (furan), $\Delta n_l(293.15\ \mathrm{K},\ 632.8\ \mathrm{nm})=1.92\times10^{-9}$ (thiophene), $\Delta n_l(293.15\ \mathrm{K},\ 632.8\ \mathrm{nm})=2.02\times10^{-9}$ (selenophene) computed *ab initio*. The calculated results also allow for a more detailed analysis of the increase in terms of variations in the properties involved in the definition of $\Delta n_l(T,\lambda)$ [see Eqs. (10), (12), and (13)]. In particular, they indicate that the largest change going from furan to thiophene is in the components of the effective electric polarizability on the molecular plane (yy and zz), and in the component of the magnetizability along the principal molecular axis. These results indicate that for furan and its homologues, thiophene and selenophene, the electronic distribution exhibits a different response behavior to the applied electric and magnetic fields, respectively. The response is more sensitive on the molecular plane for the electric perturbation and along the principal molecular axis for the magnetic one.

In order to test the stability of the solvation model we have repeated the calculations for furan in two solvents (acetone and cyclohexane) (i) neglecting the cavity field effects (see Sec. II B for details), and (ii) including solvent effects on the geometry of the solute. The results can be discussed with reference to Table VII together with Table IV. The following conclusions can be drawn.

TABLE IV. B3LYP/d-aug-cc-pVDZ and experimental results for furan in different solvents (results in a.u.). Molecule on xz plane. λ=632.8 nm.

	Acetonitrile	Acetone	Tetrahydrofuran	Cyclohexane	Dimethylformamide	CCl_4
n^2	1.806	1.841	1.971	2.028	2.046	2.129
ϵ	36.64	20.7	7.5	2.015	36.7	2.228
$\tilde{\alpha}_{xx}$	75.42	75.91	77.63	78.78	78.27	79.82
$\tilde{\alpha}_{yy}$	47.87	48.20	49.33	49.40	50.14	50.30
$\tilde{\alpha}_{zz}$	69.51	69.96	71.57	72.38	72.32	73.43
$\tilde{\alpha}_{\rm iso}$	64.27	64.69	66.18	66.85	66.91	67.85
ξ_{xx} [a]	−6.62	−6.62	−6.62	−6.62	−6.62	−6.61
ξ_{yy} [a]	−14.66	−14.66	−14.66	−14.66	−14.66	−14.66
ξ_{zz} [a]	−5.83	−5.84	−5.85	−5.89	−5.83	−5.89
$\xi_{\rm iso}$	−9.04	−9.04	−9.04	−9.06	−9.04	−9.05
$[\tilde{\alpha}\xi]$ [b]	407.50	410.07	418.57	433.08	417.05	435.84
$10^{-3}\times\tilde{Q}$(293.15 K,λ)	29.26	29.45	30.06	31.10	29.95	31.30
$\Delta\eta$	−23.75	−23.28	−21.81	−19.10	−23.75	−19.28
$10^9\times\Delta n_l$(293.15 K,λ) [c]	2.11	1.50	1.34	1.02	1.38	1.13
$10^9\times\Delta n_l$(293.15 K,λ)(exp) [c]	2.38	1.41	1.26	0.98		1.10

[a] See also Ref. 18, cited as taken from Refs. 65 and 67: in cyclohexane, $\xi_{xx}=-7.01\pm0.34$; $\xi_{yy}=-14.86\pm0.34$; $\xi_{zz}=-6.42\pm0.34$.
[b] $[\tilde{\alpha}\xi]=[(\tilde{\alpha}_{xx}-\tilde{\alpha}_{yy})\cdot(\xi_{xx}-\xi_{yy})+(\tilde{\alpha}_{yy}-\tilde{\alpha}_{zz})\cdot(\xi_{yy}-\xi_{zz})+(\tilde{\alpha}_{zz}-\tilde{\alpha}_{xx})\cdot(\xi_{zz}-\xi_{xx})]=3[\tilde{\alpha}_{xx}\cdot(\xi_{xx}-\xi_{\rm iso})+\tilde{\alpha}_{yy}\cdot(\xi_{yy}-\xi_{\rm iso})+\tilde{\alpha}_{zz}\cdot(\xi_{zz}-\xi_{\rm iso})]$.
[c] See the definition in Eq. (20).

(i) As reported in Sec. II B and as already widely recognized (see Refs. 49 and 42), the inclusion of the so-called cavity field effects in the response properties of solvated molecules is an important issue. In the present work we have used the PCM reformulation of the problem which includes cavity effects directly in the quantum-mechanical calculation of the polarizability [see Eq. (18)]. The data reported in Table VII show that the cavity field effect accounts for 16%–18% in the individual components of the polarizability tensors in both solvents but only for 2%–3% in the value of Δn.

(ii) In Table VII we also report a comparison between results obtained at the experimental geometry and those obtained at a geometry re-optimized in the solution. The effects due to geometry changes are of the order of 1% on the individual components of the polarizability, and of the order of 2.4% in cyclohexane, 2.8% in acetone when considering Δn. This shows that relaxing the geometry in the presence of the solvent induces an increase of Δn larger than that observed allowing for geometry relaxation in gas phase (≈1%–2%). The increase of Δn can be explained in terms of a differential increase in the polarizability components (around 1.5% in the xx and zz components and only 0.6% in the yy component) due to the larger bond lengths and larger angles on the xz molecular plane in the presence of the solvent.

TABLE V. B3LYP/d-aug-cc-pVDZ and experimental results for thiophene in different solvents (results in a.u.). Molecule on xz plane. λ=632.8 nm.

	Acetonitrile	Acetone	Tetrahydrofuran	Cyclohexane	Dimethylformamide	CCl_4
n^2	1.806	1.841	1.971	2.028	2.046	2.129
ϵ	36.64	20.7	7.5	2.015	36.7	2.228
$\tilde{\alpha}_{xx}$	92.69	93.33	95.62	97.07	96.51	98.47
$\tilde{\alpha}_{yy}$	61.85	62.29	63.84	63.97	65.03	65.23
$\tilde{\alpha}_{zz}$	102.58	103.29	105.80	107.03	107.00	108.70
$\tilde{\alpha}_{\rm iso}$	85.70	86.30	88.42	89.36	89.51	90.80
ξ_{xx} [a]	−8.34	−8.34	−8.35	−8.37	−8.34	−8.36
ξ_{yy} [a]	−19.43	−19.43	−19.44	−19.45	−19.43	−19.45
ξ_{zz} [a]	−8.37	−8.37	−8.39	−8.43	−8.37	−8.43
$\xi_{\rm iso}$	−12.05	−12.05	−12.06	−12.08	−12.05	−12.08
$[\tilde{\alpha}\xi]$ [b]	792.33	797.39	815.62	840.67	813.26	846.58
$10^{-3}\times\tilde{Q}$(293.15 K,λ)	56.90	57.26	58.57	60.37	58.40	60.79
$\Delta\eta$	104.16	103.99	102.59	93.06	104.16	94.25
$10^9\times\Delta n_l$(293.15 K,λ) [c]	4.12	2.92	2.62	1.99	2.69	2.19
$10^9\times\Delta n_l$(293.15 K,λ)(exp) [c]	3.67	2.63	2.31	1.92		

[a] See also Ref. 18, cited as taken from Refs. 65 and 67: in cyclohexane, $\xi_{xx}=-8.52\pm0.27$; $\xi_{yy}=-8.61\pm0.25$; $\xi_{zz}=-19.10\pm0.36$.
[b] $[\tilde{\alpha}\xi]=[(\tilde{\alpha}_{xx}-\tilde{\alpha}_{yy})\cdot(\xi_{xx}-\xi_{yy})+(\tilde{\alpha}_{yy}-\tilde{\alpha}_{zz})\cdot(\xi_{yy}-\xi_{zz})+(\tilde{\alpha}_{zz}-\tilde{\alpha}_{xx})\cdot(\xi_{zz}-\xi_{xx})]=3[\tilde{\alpha}_{xx}\cdot(\xi_{xx}-\xi_{\rm iso})+\tilde{\alpha}_{yy}\cdot(\xi_{yy}-\xi_{\rm iso})+\tilde{\alpha}_{zz}\cdot(\xi_{zz}-\xi_{\rm iso})]$.
[c] See the definition in Eq. (20).

TABLE VI. B3LYP/aug-cc-pVDZ and experimental results for selenophene in different solvents (results in a.u.). Molecule on xz plane. λ=632.8 nm.

	Acetonitrile	Acetone	Tetrahydrofuran	Cyclohexane	Dimethylformamide	CCl_4
n^2	1.806	1.841	1.971	2.028	2.046	2.129
ϵ	36.64	20.7	7.5	2.015	36.7	2.228
$\tilde{\alpha}_{xx}$	100.59	101.19	103.86	105.28	104.89	107.01
$\tilde{\alpha}_{yy}$	69.67	69.93	71.97	71.86	73.36	73.56
$\tilde{\alpha}_{zz}$	117.65	118.36	121.45	122.80	122.82	124.90
$\tilde{\alpha}_{\mathrm{iso}}$	95.97	96.49	99.09	99.98	100.36	101.82
ξ_{xx} [a]	−9.99	−9.99	−10.00	−10.02	−9.99	−10.02
ξ_{yy} [a]	−21.09	−21.09	−21.09	−21.11	−21.09	−21.11
ξ_{zz} [a]	−10.23	−10.23	−10.24	−10.28	−10.23	−10.28
ξ_{iso}	−13.77	−13.77	−13.78	−13.80	−13.77	−13.80
$[\tilde{\alpha}\xi]$ [b]	860.36	868.82	886.50	917.75	882.82	922.11
$10^{-3}\times\tilde{Q}(293.15\ \mathrm{K},\lambda)$	61.78	62.39	63.66	65.91	63.40	66.22
$\Delta\eta$	237.62	236.56	231.80	211.23	237.64	213.55
$10^9\times\Delta n_l(293.15\ \mathrm{K},\lambda)$ [c]	4.48	3.19	2.85	2.18	2.93	2.39
$10^9\times\Delta n_l(293.15\ \mathrm{K},\lambda)(\exp)$ [c]		2.81		2.02		

[a] See also Ref. 18, cited as taken from Refs. 65 and 67: in cyclohexane, $\xi_{xx}=-10.4\pm0.5$; $\xi_{yy}=-10.5\pm0.4$; $\xi_{zz}=-21.2\pm0.5$.
[b] $[\tilde{\alpha}\xi]=[(\tilde{\alpha}_{xx}-\tilde{\alpha}_{yy})\cdot(\xi_{xx}-\xi_{yy})+(\tilde{\alpha}_{yy}-\tilde{\alpha}_{zz})\cdot(\xi_{yy}-\xi_{zz})+(\tilde{\alpha}_{zz}-\tilde{\alpha}_{xx})\cdot(\xi_{zz}-\xi_{xx})]=3[\tilde{\alpha}_{xx}\cdot(\xi_{xx}-\xi_{\mathrm{iso}})+\tilde{\alpha}_{yy}\cdot(\xi_{yy}-\xi_{\mathrm{iso}})+\tilde{\alpha}_{zz}\cdot(\xi_{zz}-\xi_{\mathrm{iso}})]$.
[c] See the definition in Eq. (20).

VI. CONCLUSIONS

We have presented the theory for the quantum-mechanical calculation of the magnetic field induced birefringence (Cotton–Mouton effect) in the condensed phase within the framework of the IEF polarizable continuum model. Due to the definition of effective properties, this theory allows for the direct comparison of experimental data with the results of the quantum-mechanical calculation without the need to use scaling parameters to account for the local field effects.

We have performed an extensive study of the behavior of the furan family of homologues (furan, thiophene, and selenophene) when subject to static magnetic fields and to electromagnetic radiation both in the gas phase and in solution, by computing and at the same time in some cases measuring the resulting CME. This has permitted on one side to put to a test and evaluate the efficiency of theoretical models and computational approaches such as DFT coupled to PCM, for the accurate and cost effective determination of rather sophisticated molecular properties as electric dipole polarizabilities, magnetizabilities, and hypermagnetizabilities. On the other side it has involved the factual interplay of theory and experiment, with the exploitation of the capabilities of the experimental apparatus available nowadays for routine measurements of electromagnetic and optical properties in a wide range of conditions.

TABLE VII. B3LYP/d-aug-cc-pVDZ results for furan in cyclohexane and acetone (results in a.u.) obtained with full solvent response (1), with a reaction-field only model (2), and with optimized geometry (3). Molecule on xz plane. λ=632.8 nm.

	Acetone			Cyclohexane		
	(1)	(2)	(3)	(1)	(2)	(3)
$\tilde{\alpha}_{xx}$	75.91	66.92	76.99	78.78	68.42	79.66
$\tilde{\alpha}_{yy}$	48.20	39.58	48.53	49.40	39.57	49.67
$\tilde{\alpha}_{zz}$	69.96	60.72	70.96	72.38	61.77	73.22
$\tilde{\alpha}_{\mathrm{iso}}$	64.69	55.74	65.50	66.85	56.59	67.52
ξ_{xx}	−6.62	−6.62	−6.63	−6.62	−6.62	−6.63
ξ_{yy}	−14.66	−14.66	−14.68	−14.66	−14.66	−14.68
ξ_{zz}	−5.84	−5.84	−5.90	−5.89	−5.89	−5.94
ξ_{iso}	−9.04	−9.04	−9.07	−9.06	−9.06	−9.08
$[\tilde{\alpha}\xi]$ [a]	410.07	401.51	421.54	433.08	421.68	443.08
$10^{-3}\times\tilde{Q}(293.15\ \mathrm{K},\lambda)$	29.45	28.83	30.27	31.10	30.28	31.82
$\Delta\eta$	−23.28	−23.28	−21.60	−19.10	−18.08	−18.07
$10^9\times\Delta n_l(293.15\ \mathrm{K},\lambda)$ [b]	1.50	1.47	1.54	1.02	1.00	1.05

[a] $[\tilde{\alpha}\xi]=[(\tilde{\alpha}_{xx}-\tilde{\alpha}_{yy})\cdot(\xi_{xx}-\xi_{yy})+(\tilde{\alpha}_{yy}-\tilde{\alpha}_{zz})\cdot(\xi_{yy}-\xi_{zz})+(\tilde{\alpha}_{zz}-\tilde{\alpha}_{xx})\cdot(\xi_{zz}-\xi_{xx})]$
$=3[\tilde{\alpha}_{xx}\cdot(\xi_{xx}-\xi_{\mathrm{iso}})+\tilde{\alpha}_{yy}\cdot(\xi_{yy}-\xi_{\mathrm{iso}})+\tilde{\alpha}_{zz}\cdot(\xi_{zz}-\xi_{\mathrm{iso}})]$.
[b] See the definition in Eq. (20).

The agreement between theory and experiment is very good both in the gas and in the condensed phases. The gas-phase results in a way constitute a validation of the quality of the expansion bases employed throughout this study, and further confirm the noticeable capabilities of DFT in reproducing response properties which usually exhibit non-negligible dependence on the electron correlation.

The comparison of computed and experimental data in the pure liquids and in solution allows one to draw provisional conclusions on the use of PCM as a model for the description of the CME in the condensed phase. The combination of PCM and DFT yields excellent results for the effective isotropic electric dipole polarizabilities and magnetizabilities. More important for the scope of this paper, the present study seems to show that it is definitely possible to correctly describe anisotropic electric dipole polarizabilities and magnetizabilities and high order mixed electric and magnetic properties in solution exploiting a pure continuum model. This statement applies to systems where the interaction between the molecule whose property is under study and the medium is weak. Among the cases analyzed here there are instances (see, e.g., liquid thiophene or selenophene) where strong specific interactions appear, and where our approach appears to run into problems. It is on the other hand fair to say that perspectives for the routine computation of combined electric and magnetic properties in solutions appear to be bright.

APPENDIX: UNITS AND CONVERSIONS

Units and conversion factors are based on the recommendation given by IUPAC,[64] see also Ref. 5. Here we give explicitly the specific factors entering some of the relevant equations introduced in the body of the paper.

(1) Equations (5) and (11) (i.e., Ref. 21):

$$
\begin{aligned}
{}_mC(T,\lambda) &= 3.758\,75\times10^{-21}[\Delta\eta(\lambda)+Q(T,\lambda)] \\
&= 3.758\,75\times10^{-21} \\
&\quad\times\left[\Delta\eta(\lambda)+2.105\,16\times10^{4}\times\frac{[\alpha\xi]}{T}\right]
\end{aligned}
$$

with the quantities within the square brackets given in atomic units, gives the molar Cotton–Mouton constant directly in units of $\mathrm{cm^3\,G^{-2}\,mol^{-1}}\,(4\pi\epsilon_0)$. Above

$$
\begin{aligned}
[\alpha\xi] &= [(\alpha_{xx}-\alpha_{yy})\cdot(\xi_{xx}-\xi_{yy})+(\alpha_{yy}-\alpha_{zz}) \\
&\quad\cdot(\xi_{yy}-\xi_{zz})+(\alpha_{zz}-\alpha_{xx})\cdot(\xi_{zz}-\xi_{xx})] \\
&= 3[\alpha_{xx}\cdot(\xi_{xx}-\xi_{\mathrm{iso}})+\alpha_{yy}\cdot(\xi_{yy}-\xi_{\mathrm{iso}}) \\
&\quad+\alpha_{zz}\cdot(\xi_{zz}-\xi_{\mathrm{iso}})]
\end{aligned}
$$

and the same equation with effective properties can be employed for the condensed phase.

(2) Equations (4) and (10) [i.e., Eq. (21)]:

$$
\begin{aligned}
\Delta n_u(T,\lambda) &= \frac{\pi B^2 N_A}{V_m(4\pi\epsilon_0)}[\Delta\eta(\lambda) \\
&\quad+Q(T,\lambda)]|_{B=1\ \mathrm{T},P=1\ \mathrm{atm}} \\
&= \frac{\pi B^2 P}{kT(4\pi\epsilon_0)}[\Delta\eta(\lambda) \\
&\quad+Q(T,\lambda)]|_{B=1\ \mathrm{T},P=1\ \mathrm{atm}}, \\
\Delta n_u(T,\lambda) &= \frac{6.183\,85\times10^{-14}}{T}\times[\Delta\eta(\lambda)+Q(T,\lambda)]
\end{aligned}
\tag{A1}
$$

with the quantities within the square brackets again given in atomic units and T given in degrees kelvin.

$$
\begin{aligned}
\Delta n_l(T,\lambda) &= \frac{5.074\,31\times10^{-15}}{n}\times c^{\mathrm{pl}}_{\mathrm{solvent}} \\
&\quad\times[\Delta\tilde{\eta}(\lambda)+\tilde{Q}(T,\lambda)],
\end{aligned}
\tag{A2}
$$

which assumes once again that the quantities within the square brackets are given in atomic units and $c^{\mathrm{pl}}_{\mathrm{solvent}}$ in $\mathrm{mol\,l^{-1}}$.

(3) Also

$$
{}_mC(T,\lambda) = 7.407\,41\times10^{-16}\times\lambda\times C_{\mathrm{CM}}\times n\times\frac{1}{c^{\mathrm{pl}}_{\mathrm{solvent}}}
\tag{A3}
$$

with λ given in nm, C_{CM} given in $\mathrm{m^{-1}\,T^{-2}}$, and $c^{\mathrm{pl}}_{\mathrm{solvent}}$ given in $\mathrm{mol\,l^{-1}}$ gives again the molar Cotton–Mouton constant in units of $\mathrm{cm^3\,G^{-2}\,mol^{-1}}\,(4\pi\epsilon_0)$.

[1] A. Cotton and H. Mouton, C. R. Hebd. Seances Acad. Sci. **141**, 317 (1905).
[2] A. Cotton and H. Mouton, C. R. Hebd. Seances Acad. Sci. **141**, 349 (1905).
[3] A. D. Buckingham and J. A. Pople, Proc. Phys. Soc. London, Sect. B **69**, 1133 (1956).
[4] A. D. Buckingham, W. H. Pritchard, and D. H. Whiffen, Trans. Faraday Soc. **63**, 1057 (1967).
[5] C. Rizzo, A. Rizzo, and D. M. Bishop, Int. Rev. Phys. Chem. **16**, 81 (1997).
[6] A. D. Buckingham, Proc. Phys. Soc., London, Sect. A **68**, 910 (1955).
[7] J. H. Williams, Adv. Chem. Phys. **85**, 361 (1993).
[8] J. H. Williams and J. Torbet, J. Phys. Chem. **96**, 10477 (1992).
[9] K. Ruud, T. Helgaker, A. Rizzo, S. Coriani, and K. V. Mikkelsen, J. Chem. Phys. **107**, 894 (1997).
[10] K. Ruud, H. Ågren, P. Dahle, T. Helgaker, A. Rizzo, S. Coriani, H. Koch, K. O. Sylvester-Hvid, and K. V. Mikkelsen, J. Chem. Phys. **108**, 599 (1998).
[11] B. Mennucci, J. Am. Chem. Soc. **124**, 1506 (2002).
[12] C. Cappelli, B. Mennucci, C. O. Da Silva, and J. Tomasi, J. Chem. Phys. **112**, 5382 (2000).
[13] S. Miertuš, E. Scrocco, and J. Tomasi, Chem. Phys. **55**, 117 (1981).
[14] R. Cammi and J. Tomasi, J. Comput. Chem. **16**, 1449 (1995).
[15] E. Cancés and B. Mennucci, J. Math. Chem. **23**, 309 (1998).
[16] E. Cancés, B. Mennucci, and J. Tomasi, J. Chem. Phys. **107**, 3032 (1997).
[17] B. Mennucci, E. Cancés, and J. Tomasi, J. Phys. Chem. B **101**, 10506 (1997).
[18] G. R. Dennis, I. R. Gentle, G. L. D. Ritchie, and C. G. Andrieu, J. Chem. Soc., Faraday Trans. 2 **79**, 539 (1983).
[19] J. Kerr, Philos. Mag. **50**, 337 (1875).
[20] A. D. Buckingham, J. Chem. Phys. **30**, 1580 (1959).
[21] M. H. Coonan, I. E. Craven, M. R. Hesling, G. L. D. Ritchie, and M. A. Spackman, J. Phys. Chem. **96**, 7301 (1992).
[22] C. Cappelli, B. Mennucci, J. Tomasi, R. Cammi, and A. Rizzo, Chem. Phys. Lett. **346**, 251 (2001).

[23] R. J. W. Le Fèvre, P. H. Williams, and J. M. Eckert, Aust. J. Chem. **18**, 1133 (1965).
[24] C. G. Le Fèvre and R. J. W. Le Fèvre, J. Chem. Soc. **1953**, 4041 (1953).
[25] D. Jonsson, P. Norman, H. Ågren, A. Rizzo, S. Coriani, and K. Ruud, J. Chem. Phys. **114**, 8372 (2001).
[26] D. Jonsson, P. Norman, O. Vahtras, H. Ågren, and A. Rizzo, J. Chem. Phys. **106**, 8552 (1997).
[27] A. Rizzo, T. Helgaker, K. Ruud, A. Barszczewicz, M. Jaszunski, and P. Jørgensen, J. Chem. Phys. **102**, 8953 (1995).
[28] A. D. Buckingham, Adv. Chem. Phys. **12**, 107 (1967).
[29] M. E. Casida, in *Recent Advances in Density Functional Methods, Part I*, edited by D. P. Chong (World Scientific, Singapore, 1995).
[30] V. E. Ingamells, M. G. Papadopoulos, N. C. Handy, and A. Willetts, J. Chem. Phys. **109**, 1845 (1998).
[31] P. Calaminici, K. Jug, and A. M. Köster, J. Chem. Phys. **109**, 7756 (1998).
[32] C. Adamo, M. Cossi, G. Scalmani, and V. Barone, Chem. Phys. Lett. **307**, 265 (1999).
[33] K. Ruud, D. Jonsson, and P. R. Taylor, Phys. Chem. Chem. Phys. **2**, 2161 (2000).
[34] R. Wortmann and D. M. Bishop, J. Chem. Phys. **108**, 1001 (1998).
[35] P. Norman, Y. Luo, and H. Ågren, J. Chem. Phys. **107**, 9535 (1997).
[36] P. Macak, P. Norman, Y. Luo, and H. Ågren, J. Chem. Phys. **112**, 1868 (2000).
[37] W. Liptay, D. Wehning, J. Becker, and T. Rehm, Z. Naturforsch. A **37**, 1369 (1982).
[38] W. Liptay, J. Becker, D. Wehning, W. Lang, and O. Burkhard, Z. Naturforsch. A **37**, 1396 (1982).
[39] R. Cammi, B. Mennucci, and J. Tomasi, J. Phys. Chem. A **102**, 870 (1998).
[40] R. Cammi, B. Mennucci, and J. Tomasi, J. Phys. Chem. A **104**, 4690 (2000).
[41] S. Corni, C. Cappelli, R. Cammi, and J. Tomasi, J. Phys. Chem. A **105**, 8310 (2001).
[42] C. J. F. Böttcher and P. Bordewijk, *Theory of Electric Polarization* (Elsevier, Amsterdam, 1978), Vol. II.
[43] R. Cammi, J. Chem. Phys. **109**, 3185 (1998).
[44] M. A. Aguilar, F. J. O. del Valle, and J. Tomasi, J. Chem. Phys. **98**, 7375 (1993).
[45] R. Cammi and J. Tomasi, Int. J. Quantum Chem., Quantum Chem. Symp. **29**, 465 (1995).
[46] B. Mennucci, R. Cammi, and J. Tomasi, J. Chem. Phys. **109**, 2798 (1998).
[47] C. Cappelli, S. Corni, B. Mennucci, R. Cammi, and J. Tomasi, J. Chem. Phys. **113**, 11270 (2000).
[48] C. Cappelli, S. Corni, and J. Tomasi, J. Chem. Phys. **115**, 5531 (2001).
[49] C. J. F. Böttcher, *Theory of Electric Polarization* (Elsevier, Amsterdam, 1973), Vol. I.
[50] R. Cammi, M. Cossi, B. Mennucci, and J. Tomasi, J. Chem. Phys. **105**, 10556 (1996).
[51] J. R. Cheeseman, M. J. Frisch, G. W. Trucks, and T. A. Keith, J. Chem. Phys. **104**, 5497 (1996).
[52] T. A. Keith and R. F. W. Bader, Chem. Phys. Lett. **210**, 223 (1993).
[53] T. A. Keith and R. F. W. Bader, Chem. Phys. Lett. **194**, 1 (1992).
[54] G. Maret and G. Weil, Biopolymers **22**, 2727 (1983).
[55] T. Roth and G. L. J. A. Rikken, Phys. Rev. Lett. **88**, 063001 (2002).
[56] *CRC Handbook of Chemistry and Physics*, edited by D. R. Lide, 79th ed. (CRC, Boca Raton, FL, 1998).
[57] Sigma-Aldrich online catalogue, see http://www.sigmaaldrich.com/
[58] F. Mata, M. C. Martin, and G. O. Sorensen, J. Mol. Struct. **48**, 157 (1978).
[59] A. A. El-Azhary and H. U. Suter, J. Phys. Chem. **100**, 15056 (1996).
[60] J. S. Kwiatkowski, J. Leszczyński, and I. Teca, J. Mol. Struct. **436-437**, 451 (1997).
[61] A. Bondi, J. Phys. Chem. **68**, 441 (1964).
[62] M. J. Frisch, G. W. Trucks, H. B. Schlegel *et al.*, GAUSSIAN 01, Development Version Revision B.01, Gaussian, Inc., Pittsburgh, PA, 2001.
[63] O. Christiansen, A. Halkier, and P. Jørgensen, Chem. Phys. Lett. **281**, 438 (1997).
[64] I. Mills, T. Cvitas, K. Homann, N. Kallay, and K. Kuchitzu, *Quantities, Units and Symbols in Physical Chemistry* (Blackwell Science, Oxford, 1993).
[65] D. H. Sutter and W. H. Flygare, J. Am. Chem. Soc. **91**, 4063 (1969).
[66] K. Kamada, M. Ueda, H. Nagao, K. Tawa, T. Sugino, Y. Shmizu, and K. Ohta, J. Phys. Chem. A **104**, 4723 (2000).
[67] W. Czieslik, D. H. Sutter, H. Dreizler, C. L. Norris, S. L. Rock, and W. H. Flygare, Z. Naturforsch. Teil A **27**, 1691 (1972).